Detailed Comparisons of COMBAT Data to Wave-Optics Simulations

Richard Holmes, Jacob Lucas
Boeing LTS, 550 Lipoa Parkway, Kihei, HI, 96753
Jeremy Bos
NRC Research Associate, Air Force Research Laboratory, 550 Lipoa Parkway, Kihei, HI, 96753
V.S. Rao Gudimetla
Air Force Research Laboratory, 550 Lipoa Parkway, Kihei, HI, 96753

ABSTRACT

An experiment called COherent Multi-Beam Atmospheric Transceiver (COMBAT) collected data in 2010 along the path between Mauna Loa and Haleakala and is one of many to investigate atmospheric effects in long horizontal optical paths [1-7]. The data has proven difficult to interpret in terms of conventional analyses and wave-optics simulations. Recent modifications to the wave-optics simulations have shown better agreement with the subset of the COMBAT data that is available for comparison. These modifications include, in order of significance, (a) alternative C_n^2 profiles along the path from Mauna Loa to Haleakala, (b) turbulence inner scale effects including Hill bump [8], (c) non-Kolmogorov turbulence exponents [9], (d) spatial averaging due to the non-zero extent of camera pixels, (e) strong jitter source near transmitter, (f) anisotropy of turbulence, (g) camera saturation, and (h) camera noise. With the inclusion of these effects, quantitative agreement was obtained for several data sets for the normalized intensity variance (NIV), and for the spatial structure of intensity autocorrelations. Other properties of the data are investigated as well.

1. INTRODUCTION

Characterization of the impact of turbulence on propagation of light over long horizontal paths has had a long history [1-7]. However, early attempts at characterization did not utilize imaging detectors and so were limited to basic statistics and single-point moments. A recent attempt to improve such characterization of propagation of light is the COherent Multi-Beam Atmospheric Transceiver (COMBAT) experiment [1, 2]. Fig. 1 shows the path geometry (the left portion of the Figure is from [2]).

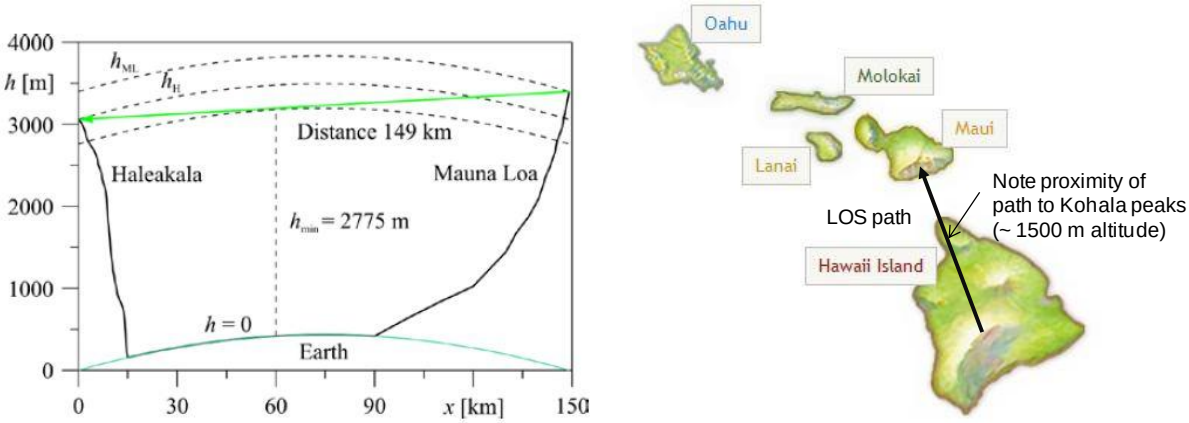

Fig. 1. Geometry of Propagation Path for COMBAT experiments.

The COMBAT experiment was intended to improve our understanding of propagation of light through deep, strong turbulence. With the 149-km path geometry shown in Figure 1, the path is definitely long, and is expected to have strong turbulence in the portions of the path over land. The data was obtained in February 2010, and in particular, the data set used herein was collected on February 17, 2010. Three laser beams at 532 nm, 1064 nm, and 1550 nm were projected from a common mount, with individual aperture diameters of 27 mm, with some divergence to ease pointing requirements to the receiver. The lasers then propagated over a path from Mauna Loa, Hawaii Island, to Haleakala, Maui Island, to the AEOS telescope. At the AEOS telescope [1]. The light received at the pupil plane

was imaged onto three cameras, one for each of the three wavelengths. The three cameras recorded images in circular regions of 90 cm in diameter within the 3.63 meter pupil of the AEOS telescope. The frame rates of the cameras were all 200 Hz, and the pixel sizes of the cameras were slightly larger than 3.5 mm, mapped to the pupil plane.

This experiment produced several results that were not expected. First, spatial scintillation, as measured by normalized intensity variance (NIV) increased markedly with increasing wavelength. Note that NIV is defined as

$$\mathrm{NIV} = \langle (\langle I^2 \rangle_f / \langle I \rangle_f^2 - 1) \rangle_t \qquad (1)$$

where I is the intensity measured at a pixel, the subscript "f" refers to an average over a single frame, and the subscript "t" refers to an average over time. This marked increase of NIV with wavelength is inconsistent with the weak-turbulence theory, which predicts that NIV should decrease with wavelength, as well the strong-turbulence theory which predicts that NIV should increase very weakly with wavelength. Second, the scale size of scintillation is from about 0.7 to 3 cm, depending on wavelength. Weak-turbulence theory predicts that the scale size should be about (Wavelength x Range)$^{1/2}$ which is 30 to 50 cm in the case of COMBAT [10-12]. Additionally, the normalized standard deviation over time of the total signal per frame, σ_{TotSig}, is quite large, from 1 to 2. This is larger than expected, as discussed in more detail below. These three issues are addressed in this paper. In the process, other interesting attributes of the data emerged.

2. REVIEW OF THE DATA

Sample frames of data are shown in Figure 2. Each column shows sample frames for a given wavelength.

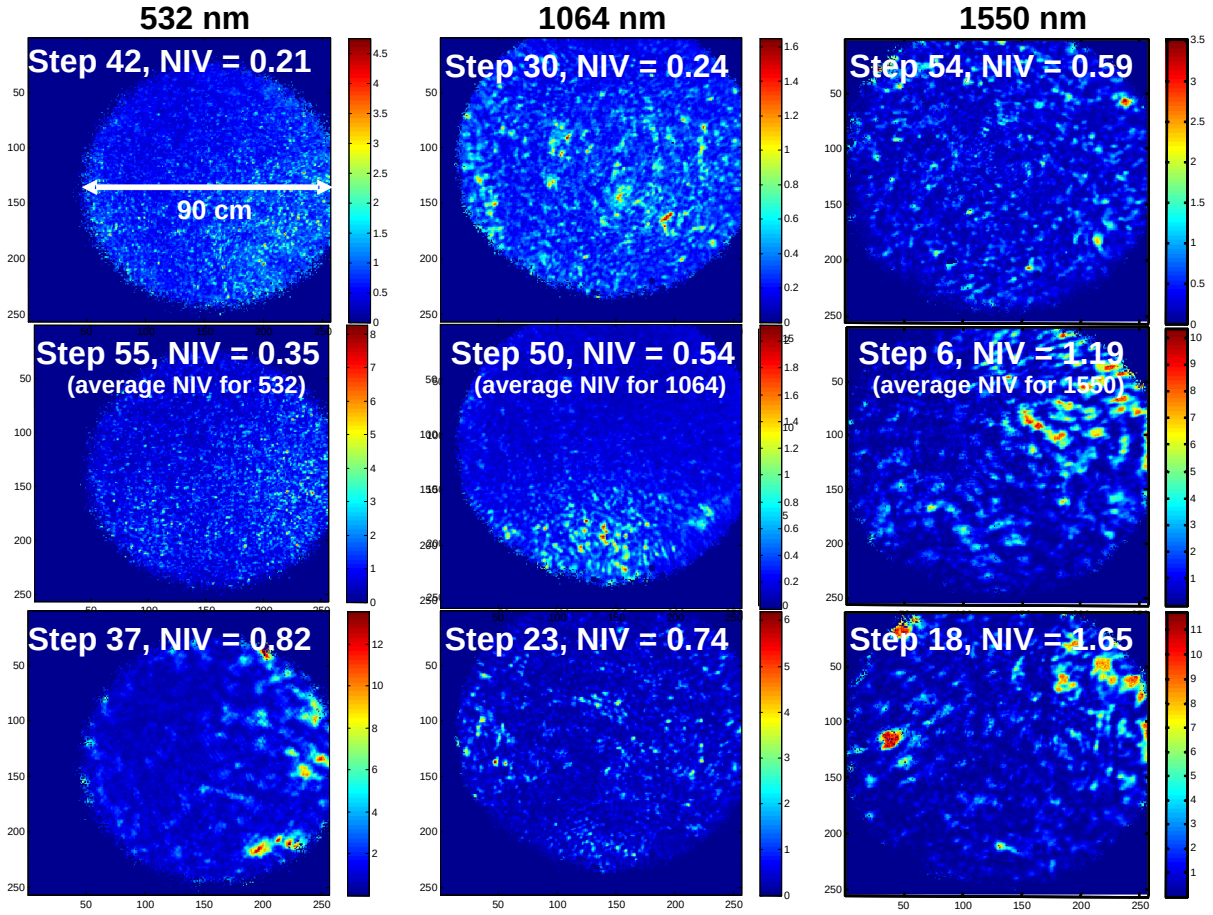

Fig. 2. Sample frames of pupil-plane data for each of the three wavelengths.

The middle row shows sample frames that have the average NIV for each wavelength. The upper and lower rows show frames with excursions of NIV about the mean, for each wavelength. Several key features should be noted. First, there are only a few bright regions in the data. Second, the scale size of the scintillations varies from less than 1 cm to 3 cm, based on the wavelength. This is much smaller than the expected scale size of a Fresnel zone, $(\lambda R)^{1/2}$, where λ is the wavelength and R is the total range, as mentioned above. The Fresnel zone is about 28 cm for a wavelength of 532 nm, and about 48 cm for 1550 nm. One can observe some structure at this scale size in the data, but it is not a dominant feature, and the intensity autocorrelations show that the finer scale of a few cm is indeed dominant. This vast difference between predicted and observed scale size is not improved significantly if one considers strong turbulence theory, which gives a scale size of about 20 cm, assuming a uniform distribution of turbulence along the path [12-14]. Also, it is worth noting that wind-based smearing of the scintillation is not evident, the scintillations would appear as streaks if this were the case.

Fig. 3 shows the temporal variation of the total signal for all three of the wavelengths' apertures. The figure also shows the standard deviation of the total signal, σ_{TotSig}, for each of the three wavelengths. It should be noted that the temporal variations do not appear to be correlated between wavelengths.

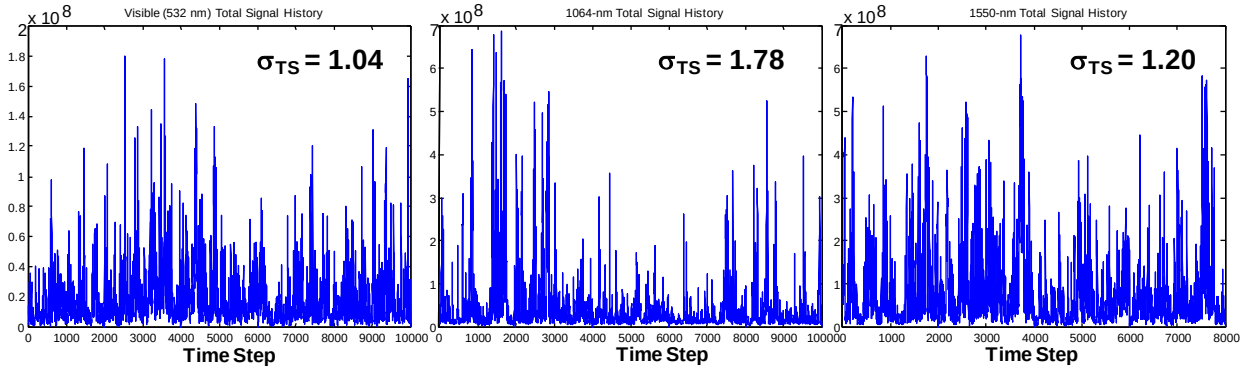

Fig. 3. Temporal variation of the total signal for all three of the wavelengths.

It can be seen that the normalized standard deviation over time of the total signal per frame, σ_{TotSig}, is quite large, from 1 to 2. This is larger than expected. Based on scintillation only, σ_{TotSig} should be no more than 0.45, because the total signal should vary as the (number of scintillation scale sizes within the aperture)$^{-1/2}$, so $\sigma_{TotSig} \sim 1/$(# of scintillation zones in 90 cm aperture)$^{1/2} \sim 1/(90^2/40^2)^{1/2} = 0.45$. Based on this, scintillation is *not* the primary cause of variations in total signal. Hence, a more likely explanation is that transmitter jitter or strong turbulence near the transmitter causes of the large temporal variation of total signal. It's worth observing the time histories of the jitter in Fig. 3 do not show any significant correlation. Hence, a working hypothesis is that the jitter is not caused by the transmitter telescope, but by whole-beam jitter due to strong turbulence near the transmitter. Another possibility is that transmitter jitter is the cause and the individual beams have some relative boresight error, so that when one beam is high on the receiver, the other beam(s) are low.

Fig. 4 is useful in identifying the source of the large variations in the total signal. This figure shows the power spectral density of the total signal variations. The power-law observed is -2 ± 0.2, and this is a signature for turbulence-induced jitter rather than telescope jitter or scintillation. This differs from the scintillation power spectral density (PSD), which should fall off as $f^{-8/3}$, and aperture averaging of the scintillation should give an even steeper fall-off with frequency. The PSD of mechanical jitter usually falls off as f^{-4}, since I $d^2\theta/dt^2$ = torque, where I is the transmitter telescope moment of inertia and θ is the rotational angle of the telescope structure, so that $\theta \sim f^{-2}$, and $<\theta^2> \sim f^{-4}$. Hence, based on the PSD, one surmises that it is turbulence-induced jitter, and in particular jitter near the receiver to cause the large-scale fades over time.

Fig. 5 shows a sample spatial autocorrelation of the intensity measured on the camera plane. One can see a minimum in the autocorrelation which occurs near 40 cm, which is close to the Fresnel zone scale size of ~ 40 cm (as it should be, based on scintillation theory). Also, one may observe that the central correlation spike has a half width of < 1 cm in this data set, consistent with earlier remarks.

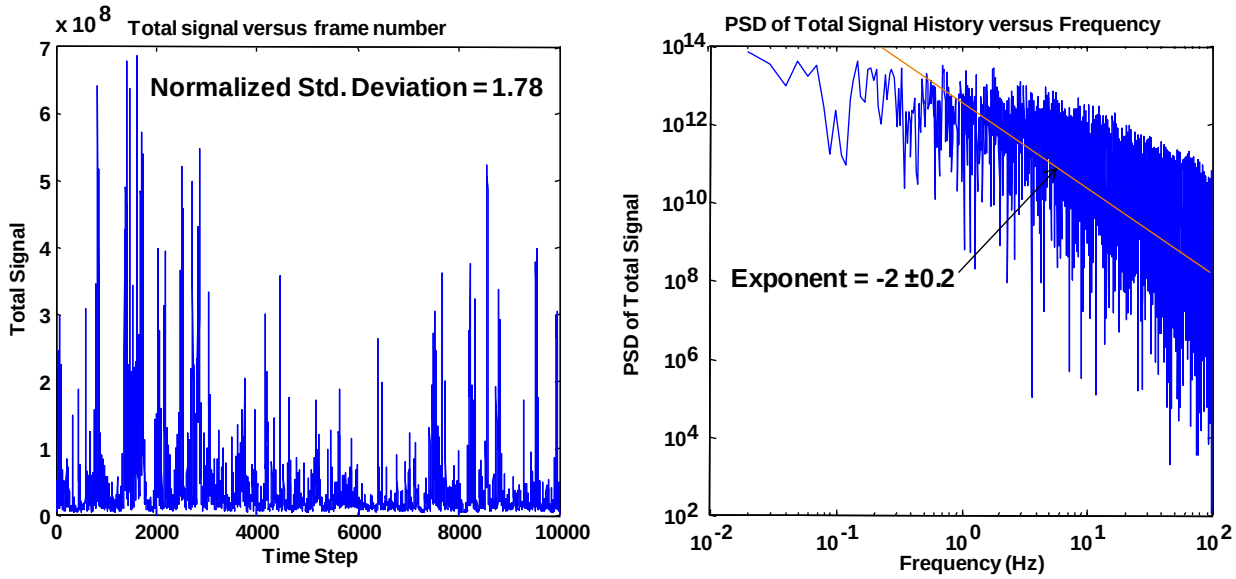

Fig. 4. Temporal variation of the total signal for 1064 nm (left) and corresponding power spectral density (right).

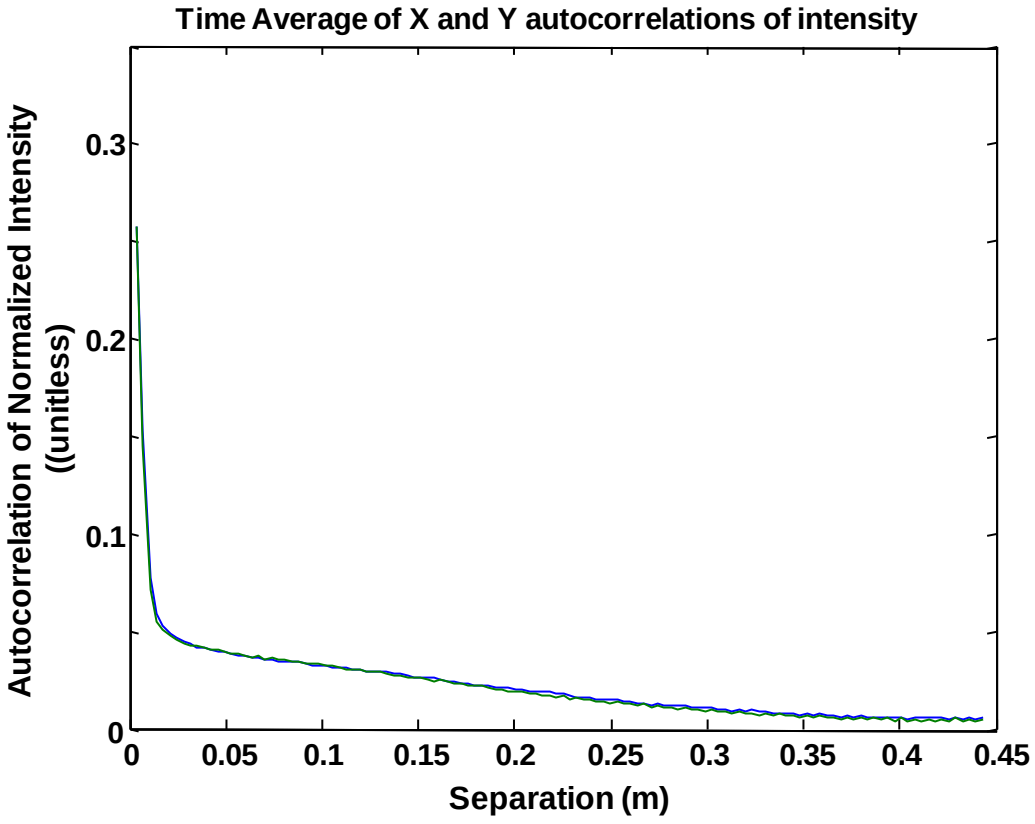

Fig. 5. Sample autocorrelation of the full data set at 532 nm (10^4 frames at 200 Hz frame rate).

Other attributes of the data were also investigated, including time histories of the NIV, histograms of the frame-by frame NIV, histograms of the signals at the pixel level, and intensity autocorrelations in time and space. Also, it should be noted that meticulous care was devoted to proper analysis of the data. For a more complete discussion of such analysis of strong scintillation data, as is needed for strong-turbulence fluctuations, see [6].

3. APPROACH

To address the 3 key unexpected findings in the data, as well as other attributes of the data, a detailed simulation was performed. The simulation included effects not normally considered, based on inspection of the above data. These effects are listed below, along with the rationale to include them.

(a) Alternative C_n^2 profiles along the path from Mauna Loa to Haleakala. Rationale: the observed small-scale turbulence is usually caused by turbulence close to the receiver. Also, one might expect that the portions of the propagation path over the lava fields of Maui and Hawaii would have stronger turbulence and paths over the ocean would have weaker turbulence. There are ways to extract C_n^2 estimates directly from data [15], but these are impractical due to strong turbulence in this case.

(b) Turbulence inner scale effects, including Hill bump. Rationale: Fine scale scintillation is observed, finer than 1 cm, which might be explained by a Hill turbulence bump at the inner scale [8].

(c) Non-Kolmogorov turbulence exponents. Rationale: it was found that the nominal Kolmogorov exponent does not match the scale sizes observed in the data, even with extreme values of C_n^2. More plausible C_n^2 values can be used if non-Kolmogorov exponents are selected.

(d) Spatial averaging due to the finite extent of the pixels. Rationale: Fine scale scintillation is observed in the data, on the order of the pixel width as mapped to the pupil (3.6 mm), hence some scintillation may be washed out within pixels. This could also help account for the trends in NIV, if smaller-scale scintillation is filtered out by the pixels at the shorter wavelength.

(e) Relatively strong jitter sources near transmitter (atmosphere or telescope). Rationale: Turbulence-induced scintillation alone does not explain the large variations in total signal that is observed.

(f) Camera noise. Rationale: Camera noise is known to cause measurable scintillation on a camera, especially in cases of low signal.

(g) Camera saturation. Rationale: Camera saturation was observed in about 10% of the frames at 1064 and 1550 nm.

(h) Anisotropy of turbulence. Rationale: Anisotropy was clearly observed in about 10% of the frames at both large and small scale sizes of scintillation.

Review of the data and the simulations indicate that (a) –(f) of the above are needed to get best agreement with the data, including the "unexpected properties" of the data. Fig. 6 shows the basic parameters used in the simulations presented herein. It should be mentioned that several other parameters were used or varied. An inner-scale Hill bump was not always used, but when it was, a 3 mm inner scale was used. Also, anisotropy was used on occasion as will be seen below in the results. Also, time histories were considered. When uncorrelated frames were desired, time steps of 0.2 seconds were used, corresponding to a shift of 1 meter for most of the phase screens, with the Bufton wind model. When temporally-correlated frames were desired, in order to match the data, the same frame rate as the data collection was used (5 msec). To test the accuracy of the simulation, sometimes 2048x2048 grids were used instead of 1024x1024 grids. In such cases, a correspondingly smaller grid spacing of 0.6 mm was used, although in most cases the nominal grid spacing of 1.2 mm was used. It will be noted if a case was run with a finer resolution and more points. The standard split-step operator is used, with Fresnel propagation implemented between phase screens. The number of phase screens was varied up by a factor of two and changes in the NIV were within the randomness expected due to phase screen realizations (6-11%) when increasing the number of screens from nominal (60) to the higher number (120).

To understand the basic strength of turbulence, estimates of the key turbulence parameters are shown in Table 1, using weak-turbulence formulae, as is customary. Table 1 assumes turbulence profile (a), which is the standard Maui3 model. For turbulence profile (b), using HV 5/7 above land, and the 0.01 x Maui3 is used over water, wherein the height above the local ground level is fed into the Maui3 model, and then an adjustment is made for the density of local ground. So for example, in the middle of the path, the path height of about 2800 meters is input into the Maui3 model, and the resulting C_n^2 strength is increased by the density ratio ρ(0 meters AMSL)/ρ(3060 meters AMSL for Maui site) and multiplied by 0.01. The NIV numbers are about 6x larger for profile (b) than those for the nominal profile (a). The weak-turbulence calculations of Table 1 indicate that the turbulence is definitely strong and deep, since the NIV values are all much greater than 1.

Parameter	Value
Path Length (km)	149
Turbulence	see right
Number of Phase Screens	60 along path
Grid size (pts)	1024x1024, also 2048x2048
Grid point spacing (m)	1.2 mm (3 grid points/pix)
Turbulence type	Kolmogorov exponents of 22/6 and 19/6
Receiver Aperture Diam (m)	0.9
Camera Pixel width (mm)	3.6 mm in output space in pupil
Camera Noise	Shot noise + 1 pe rms per pixel
Number of realizations	3 per wavelength
Wavelengths (nm)	532, 1064, 1550
Propagation Divergence	Spherical

Hill Bump (inner scale 3 mm) and Anisotropy (ε=1) used in some cases.

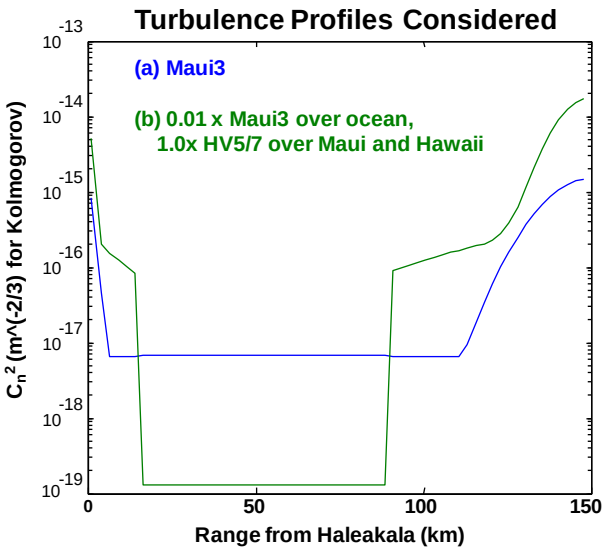

Fig. 6. Input parameters for the simulation, including turbulence strength versus range from receiver.

Table 1. Summary of key turbulence parameters for the propagation path, assuming Maui3, scaled for local density, based on weak-turbulence theory.

Parameter/λ	532 nm	1064 nm	1550 nm
Spherical r0 (cm)	4.0	9.3	14.5
Isoplanatic Patch Angle (μradians of angle)	0.03	0.07	0.11
NIV (unitless) (*)	16.0	7.1	4.6

(*) From weak perturbation theory. NIV is derived from 4 x Rytov variance.

To conclude this section, two other key comments are in order. First, simulation is the tool of choice in this investigation, since analyses have difficulty matching all the nuances of the turbulence path and the transmitter and receiver hardware details. Second, many other turbulence profiles were considered, but the corresponding results are not shown herein to simplify the presentation. Such other turbulence profiles were important in finding a reasonable match with the data.

4. SUMMARY OF COMPARISON BETWEEN DATA AND SIMULATION

The comparison between simulation and data was manifold. The key parameter, NIV, is compared in Table 2. The spatial autocorrelation of the intensity, as measured on the camera plane, is compared in Figure 7. Comparisons were also performed of the temporal autocorrelation of the intensity. Because of the unknown and variable winds along the path, the degree of agreement between the data and the simulation was not expected to be good for the temporal autocorrelation. Despite this expectation, it can be said that the agreement was fair (but is not shown).

Table 2 shows the measured NIV at each wavelength along the top row; the subsequent rows show NIV's for the three different wavelengths under different simulation conditions. The green bar on the right-hand side shows the best match of simulation NIV to measured NIV. The relative difference between the data and the sim in NIV for this best profile (C_n^2 profile (b) with Hill bump and non-Kolmogorov turbulence) is 7.5%, +60.5%, and 0%, for 532 nm, 1064 nm, and 1550 nm, respectively.

It should be noted that camera saturation (not included in this set), was clearly present in the 1064 and 1550 nm data. To investigate the impact of saturation, the data was processed in two different ways. The first approach discarded frames that had any points which equaled the saturation value. This approach is the nominal approach used in reducing the data. The second approach discarded frames that had any points which equaled or exceeded 80% of the saturation value. This choice is based on the fact that camera blooming was observed when near saturation. With this second approach the estimated NIV could be as much as about 10% lower than the NIV estimated with the nominal approach. So for example, an NIV of 0.53 was estimated using the nominal approach for the 1064 data, but was 0.48 when using the second approach for saturation. The estimated NIV for the 1550 nm data was actually about 2% higher when using the second approach.

Figure 7 shows relatively good agreement between the measured and simulated spatial autocorrelation at 532 nm. The agreement was actually better than this at the other wavelengths. Between Table 1 and Figure 7, there is cause for claim that good agreement can be found between measured data and simulations. This is confirmed qualitatively by comparison of the measured images such as in Figure 2 and the simulated images (not shown herein).

Table 2. Measured and simulated normalized intensity variance.

Wavelength → Conditions ↓	532 nm	1064 nm	1550 nm
2/17/2010 Data Set 3, Meas'd	**0.35**	**0.53 (*)**	**1.19 (*)**
Baseline Sim (profile a)	2.19	1.77	1.59
(a) With Hill Bump and Non-Kolmogorov	1.01	1.34	1.37
2*(a) With Hill Bump and Non-Kolmogorov	0.70	1.11	1.33
Modified Cn2 (profile b)	2.20	2.36	2.22
(b) With Hill Bump	1.27	2.16	1.96
(b) With Hill Bump and Non-Kolmogorov	0.376 (**)	0.85	1.19
(b) With Hill Bump, Non-Kolmogorov, and anisotropy	0.372 (**)	0.84	1.25

(*) Some camera saturation was observed at 1064 and 1550 nm.
(**) Some evidence of aliasing was present at the nominal grid point spacing, so finer grid point spacings were used as discussed in text.

5. CONCLUSIONS

The COMBAT experiment measured spatial profiles of pupil-plane scintillation at 3 different wavelengths. To obtain agreement between simulation and data for key metrics at the three wavelengths, the simulation required a C_n^2 model with strong turbulence over land close to the transmitter and receiver. The required turbulence proved to be 1 x HV 5/7, which is plausible for propagation at an elevation over lava-rock fields.

The unexpected behavior of strongly-increasing NIV versus wavelength, counter to both weak and strong turbulence theory, can be matched in simulation using a combination of C_n^2 profile, non-Kolmogorov exponent, non-uniform turbulence, and a camera model. The most important element of the camera model is the non-zero width of the pixel. Without the use of a non-Kolmogorov exponent, the turbulence strengths required became implausibly large.

The temporal variance of the measured total signal is not readily explicable by scintillation alone. Whole beam motion is required to explain the statistics of whole-aperture fades, and the measured power spectrum is consistent

with significant turbulence-induced whole-beam jitter near the transmitter. This consistency is obtained both in terms of the large magnitude of total signal variance, and the power spectrum.

In summary, both experiment and simulations indicate that imaging or data links at low elevation angles will not always perform as predicted by existing weak-turbulence theory or by the limited strong-turbulence theory that is currently available. On the other hand, detailed simulation of the transmitter, atmosphere, and receiver can improve agreement and predictive capability significantly. Given the wide variability of conditions observed in the data, it is recommended that any simulation treatment for performance prediction should include multiple realizations and variation of the input turbulence strength.

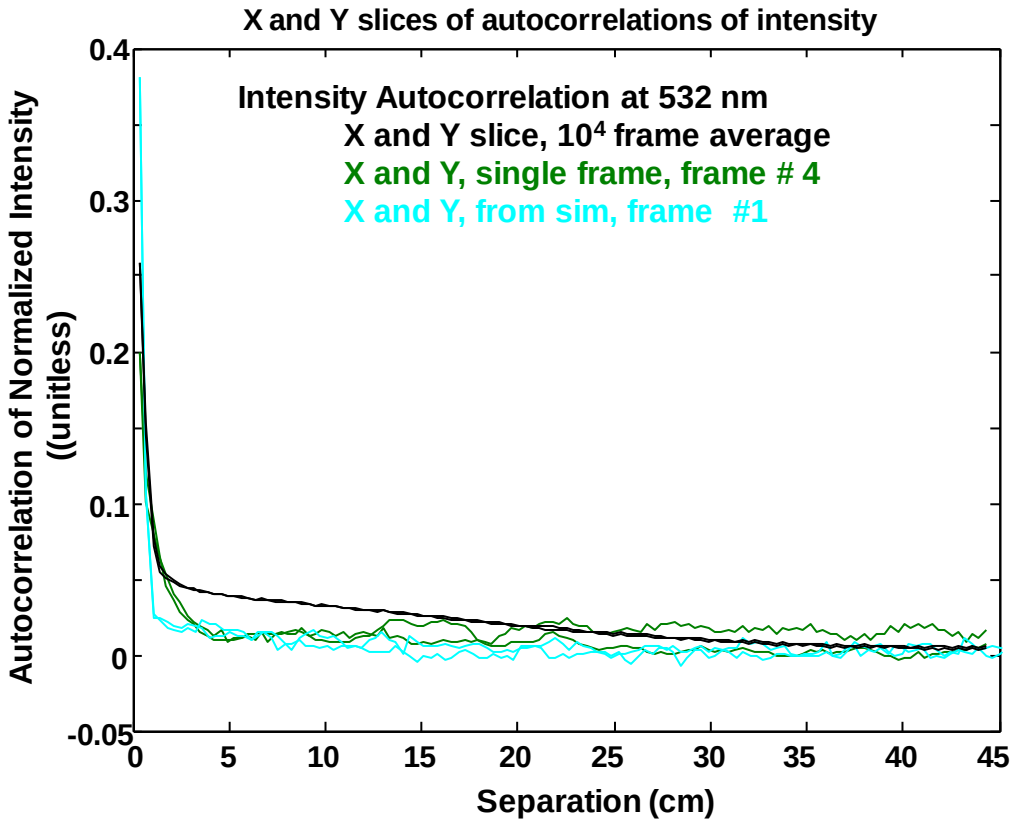

Fig. 7. Measured and simulated intensity autocorrelations – exemplary comparison at 532 nm.

6. ACKNOWLEDGMENT

This work was funded as a Laboratory Research Initiation Request by Air Force Office of Scientific Research (AFOSR) under agreement number FA9451-05-C-0257, with Rao Gudimetla as principal investigator. The U.S. Government is authorized to reproduce and distribute reprints for Governmental purposes notwithstanding any copyright notation thereon. The views and conclusions contained herein are those of the authors and should not be interpreted as necessarily representing the official policies or endorsements, either expressed or implied, of the Air Force Research Laboratory or the U.S. Government.

7. REFERENCES

1. M. A. Vorontsov, G. W. Carhart, V. S. Rao Gudimetla, T. Weyrauch, E. Stevenson, S. L. Lachinova, L. A. Beresnev, J. Liu, K. Rehder, and J. F. Riker, "Characterization of atmospheric turbulence effects over 149 km propagation path using multi-wavelength laser beacons," in *Proceedings of the 2010 AMOS Conference*, S. Ryan, ed., p. E18, 2010.

2. M. Vorontsov, V. S. Rao Gudimetla, G. Carhart , T. Weyrauch, S. Lachinova, E. Polnau, J. Reierson, L. Beresnev, J. Liu, and J. F. Riker "Comparison of turbulence-induced scintillations for multi-wavelength laser beacons over tactical (7 km) and long (149 km) atmospheric propagation paths," ," in *Proceedings of the 2011 AMOS Conference*, S. Ryan, ed., 2011.
3. G. R. Ochs, R. R. Bergman, and J. R. Snyder, "Laser-beam scintillation over horizontal paths from 5.5 to 145 kilometers," *J. Opt. Soc. Am.* Vol. 59, 231–234, 1969.
4. M. E. Gracheva, A. S. Gurvich, S. S. Kashkarov, VI V. Pokasov, "Similarity relations and their experimental verification for strong intensity fluctuations of laser radiation," in *Laser Beam Propagation in the Atmosphere*, J. W. Strohbehn, ed., 107-127, 1978.
5. N. Perlot, D. Giggenbach, H. Henniger, J. Horwath, M. Knapek, and K. Zettl, "Measurements of the beam-wave fluctuations over a 142 km atmospheric path," *Proc. SPIE* 6304, 63041O , 2006.
6. William M. Hughes and Richard B. Holmes, "Pupil plane imager for scintillometry over long horizontal paths," *Appl. Opt.* 46, pp. 7099-7109, 2007.
7. A. S. Gurvich, M. E. Gorbunov, O. V. Fedorova, G. Kirchengast, V. Proschek, G. González Abad, and K. A. Tereszchuk, "Spatio-temporal structure of a laser beam over 144 km in a Canary Islands experiment," *Appl. Opt.* 51, 7374–7383, 2012.
8. R. J. Hill and S. F. Clifford. "Modified spectrum of atmospheric temperature fluctuations and its application to optical propagation," *J. Opt. Soc. Am.* Vol. 68, 892-899, 1978.
9. V. S. Rao Gudimetla, Richard B. Holmes, Jim F. Riker, "Analytical expressions for the log-amplitude correlation function for spherical-wave propagation through anisotropic non-Kolmogorov refractive turbulence," *J. Opt. Soc. Am.* A, Vol. 31, 148–154, 2014.
10. Albert D. Wheelon, *Electromagnetic Scintillation, Vol. 1 (Geometrical Optics)*, Cambridge University Press, Cambridge, 2001.
11. L. C. Andrews and R. L. Phillips, *Laser Beam Propagation through Random Medium*, SPIE Press, Bellingham, WA, 2005.
12. A. S. Gurvich and V. I. Tatarskii, "Coherence and intensity fluctuations of light in the turbulent atmosphere," *Radio. Sci*. Vol. 1, 3-14, 1975.
13. V. P. Aksenov, K. S. Gochelashvily, V. I. Shishov, "Spatial Spikes of Laser Irradiance propagating over large distances in a turbulent medium," *Appl. Opt.* Vol. 15, 1172-1177, 1976.
14. V. S. Rao Gudimetla, Richard B. Holmes, Thomas C. Farrell and Jacob Lucas, "Phase Screen Simulations of Laser Propagation through non-Kolmogorov Turbulence," *Proc. SPIE* 8038, 803808, 2011.
15. Richard B. Holmes and William M. Hughes, "Pupil plane imager for estimation of turbulence over long horizontal paths," *Applied Optics* Vol. 46, 5979-5986 , 2007.